

# Seismic site classification from HVSR data using the Rayleigh wave ellipticity inversion: A case study in Singapore

Shynggys Abdialim<sup>1a</sup>, Farkhod Hakimov<sup>2b</sup>, Jong Kim<sup>1c</sup>, Taeseo Ku<sup>3d</sup> and Sung-Woo Moon<sup>\*1</sup>

<sup>1</sup>Department of Civil and Environmental Engineering, School of Engineering and Digital Sciences, Nazarbayev University, Kabanbay Batyr Ave. 53, Nur-Sultan 010000, Kazakhstan

<sup>2</sup>RWTH Aachen University, Neotectonics and Natural Hazards, Lochnerstraße 4–20, 52056 Aachen, Germany

<sup>3</sup>Department of Civil and Environmental Engineering, National University of Singapore, 1 Engineering Drive 2, Singapore, 117576

(Received April 6, 2021, Revised June 9, 2021, Accepted June 10, 2021)

**Abstract.** Shear wave velocity ( $V_s$ ) profile is one of the critical geotechnical measurements of soil layers for seismic hazard assessment and liquefaction potential evaluation. Enhancing the effectiveness of in-situ  $V_s$  profiling by reducing time and cost is of great interest. For that reason, this study aims at assessing  $V_s$  profile generation from a single-station three-component geophone with additional borehole log data for constraining parameter space. Based on multichannel analysis of surface waves (MASW), and microtremor array Measurements (MAM) conducted previously at seven sites located in Bukit Timah Granite, Singapore, this study utilized HVSR signals for Rayleigh wave ellipticity (ellipticity curve) inversion with additional inversion constraint using borehole log data. The resulting  $V_s$  profiles and reference  $V_s$  profiles from MASW and MAM were quantitatively compared using average  $V_s$  of 30 m ( $V_{s30}$ ). The profiles generated from ellipticity curve inversion revealed a good agreement with  $V_s$  reference profiles.  $V_{s30}$  based site classification results also indicated a good fit of two test results. Therefore, HVSR measurements for further ellipticity curve inversion, with already available borehole log data for constraint, is considered as a promising cost and time-effective site classification approach.

**Keywords:** ellipticity curve; HVSR; shear wave velocity; site classification; surface waves

## 1. Introduction

To assess the subsurface strata, usually, traditional log tests are conducted which involve site drilling, soil sampling, and further conductance of laboratory tests using the sample (Hobiger *et al.* 2013, Moon *et al.* 2016). Borehole logging can be expensive, take a huge amount of time, and inevitably cause an environmental effect due to the invasive nature (Hobiger *et al.* 2013, Moon *et al.* 2019). Boreholes can be used to explore soil properties at exact locations, and as a point of interest gets far apart from the explored location, the gathered soil property information becomes less reliable. As an alternative for borehole logging, geophysical surface wave investigation approaches sometimes can be employed. Surface wave methods are nowadays a promising approach for (1) the identification of  $V_s$  profiles of the site, and (2) characterization of geotechnical properties of tested sites utilizing dispersive behavior of surface waves (Moon *et al.* 2016, Moon and Ku 2016a, Moon and Ku 2016b, Moon *et al.* 2017, Moon and Ku 2018).

Geophysical tests such as multichannel analysis of

surface waves (MASW), microtremor array measurements (MAM), and horizontal to vertical spectral ratio (HVSR) tests would be considered as: (1) a better option over borehole log (Moon *et al.* 2017, Moon *et al.* 2019), (2) an alternative way for site response evaluation (Bonnetfoy Claudet *et al.* 2006), and (3) site classification (Pavel and Vacareanu 2015). Each of these tests has its own limitations like allowable survey depth, sharpness of resulting  $V_s$  profile, and effects of environmental noise type, underground utilities, and water. However, in a highly urbanized zone like Singapore, the application of geophysical tests is more preferred due to portability, which helps to reduce potential risk to underground utilities during tests.

Previously, Singapore geology was explored using MASW, MAM, and HVSR tests for evaluating the application of tests in local rock formations (Moon *et al.* 2016; Subramaniam *et al.* 2019) and surveying the weathering of decomposed granite (Moon *et al.* 2017; Moon and Ku 2017). For geotechnical design, local rock in accordance with (1999) is classified as “Grade III (G III)” that is based on weathering degree of a rock formation (see Table 1). Results of those studies were utilized for surveying of soil/rock interface (Ku *et al.* 2020) providing empirical approaches of estimating soil/rock interface based on  $V_s$  profiles and proposing a local power function from HVSR results that expresses the correlation between the fundamental frequency of site and the depth of soil/rock interface for Bukit Timah Granite (Moon *et al.* 2019).

Inversion of ellipticity of the fundamental mode of

\*Corresponding author, Ph.D. Assistant Professor

E-mail: sung.moon@nu.edu.kz

<sup>a</sup>Master Student

<sup>b</sup>Ph.D. Student

<sup>c</sup>Professor

<sup>d</sup>Assistant Professor

Table 1 Bukit Timah Granite rock classification based on weathering degree (1999)

I	Intact strength, unaffected by weathering. Not broken easily by hammer rings when struck. No visible discoloration.
II	Not broken easily by hammer – rings when struck. Fresh rock colors are generally retained but stained near joint surfaces.
III	Cannot be broken by hand. Easily broken by a hammer. Makes a dull or slight ringing sound when struck with a hammer. Stained throughout.
IV	Core can be broken by hand. Does not slake in water. Completely discolored.
V	Original rock texture preserved, can be crumbled by hand. Slakes in water. Completely discolored.
VI	Original rock structure completely degraded to soil, with none of the original fabric remains. Can be crumbled by hand.

Rayleigh wave (ellipticity curve), which is estimated from HVSR measurements, is generally considered as an unconventional geophysical surface wave analysis method that could be implemented in cities with highly limited space because it requires only one geophone (Hobiger *et al.* 2013). In previous studies, a group of Vs profiles generated by scaling each other has resulted from an identical ellipticity curve (Dal Moro 2011, Hobiger *et al.* 2013). To prevent the non-uniqueness of the inversion solution, it needs to be further constrained by additional geophysical or geotechnical data. Due to the demand for additional constraints, it is not clear yet whether ellipticity curve inversion is a well-recognized and reliable method to generate a reasonable Vs profile in practice. In this study, single three-component 4.5 Hz geophones and a Geometrics seismograph were utilized to record ambient noise near the seven test sites for 30 min each. Measurements are used for generating Vs profiles and further site classification by average Vs values in accordance with National Earthquake Hazard Reduction and Prevention (NEHRP) recommendations (BSSC 2001). This paper aims to generate Vs profiles for shallow depths using ellipticity curve inversion and assess its credibility by comparing soil/rock interface from Vs profile, and  $V_{S30}$  site classification.

## 2. Testing location and geology

The geology of Singapore island consists of four rock types such as volcanic rocks, sedimentary rocks, Quaternary store, and late alluvial store. Among the listed rock types, Jurong and Bukit Timah Granite formations consist of about 2/3 of the total Singapore territory. Bukit Timah formation is considered as a basal bedrock forming Singapore island due to its location below other rock formations. Due to the tropical climate of the island, heavy rains, and the presence of organic components in soil, the Bukit Timah Granite development's weathering condition varies significantly from weathered soil to hard rock layers in different locations (Ku *et al.* 2020). Geophysical methods such as multichannel analysis of surface waves (MASW), and microtremor array measurement (MAM) were

Table 2 Testing location and corresponding invasive and non-invasive data

Site ID	Testing location	Borehole	Test method	Array size (m)
S1	Ang Mo Kio Park	B1	MAM	30 x 30
			MASW	34.5
			HVSR	-
S2	And Mo Kio St. 24a	B2	MAM	40 x 40
			HVSR	-
S3	And Mo Kio St. 24b	B3	MAM	40 x 40
			HVSR	-
S4	Woodlands Ave 1a	B4	MAM	50 x 50
			MASW	46
			HVSR	-
S5	Woodlands Ave 1b	B5	MAM	50 x 50
			MASW	46
			HVSR	-
S6	Woodlands Dr. 19	B6	MAM	40 x 40
			HVSR	-
S7	Woodlands St 81	B7	MAM	30 x 30
			HVSR	-

conducted by (Moon *et al.* 2019) in Bukit Timah Granite territory. Locations where the HVSR test was conducted, and previous tests' array sizes can be seen in Table 2.

## 3. Methods

### 3.1. Multichannel Analysis of Surface Waves (MASW) and Microtremor Array Measurements (MAM)

MASW and MAM (also called Passive MASW) are geophysical surface wave methods developed specifically for subsurface purposes (Park *et al.* 1999). This method quickly became popular among geophysicists and civil engineers; it provides a subsurface wave that can give a 1D or 2D Vs profile, which is one of the most important geotechnical parameters in seismic engineering. The MASW and MAM tests are designed for high-frequency and low-frequency recordings, respectively, and subsequently investigate shallow and deep ground characteristics. The procedure in both cases consists of 1) data acquisition, 2) data processing, and (3) inversion. MASW test utilizes artificial noises like an explosion, or a sledgehammer shot generated at a certain distance away (called offset) from a linear spread of signal receivers in data acquisition. To increase the quality and sharpness of gathered data, several subsequent sledgehammer shots are usually recorded. All the received signals are then utilized for plotting the dispersion curve, Rayleigh wave velocity vs frequency curve with maximum magnitude in frequency spectra. MAM test is aimed at recording natural ambient noises, and receivers are placed at isotropic geometric shape or "L" shape. Ambient noises' source and direction are usually unknown. Data processing will result in generating the dispersion curve at lower frequency ranges.

Previously, for the Bukit Timah Granite in Singapore, dispersion curves were derived using a phase shift stack method for MASW and Spatial Autocorrelation (SPAC) (Aki 1957) or cross-correlation (Zhang *et al.* 2019, Zhang *et*

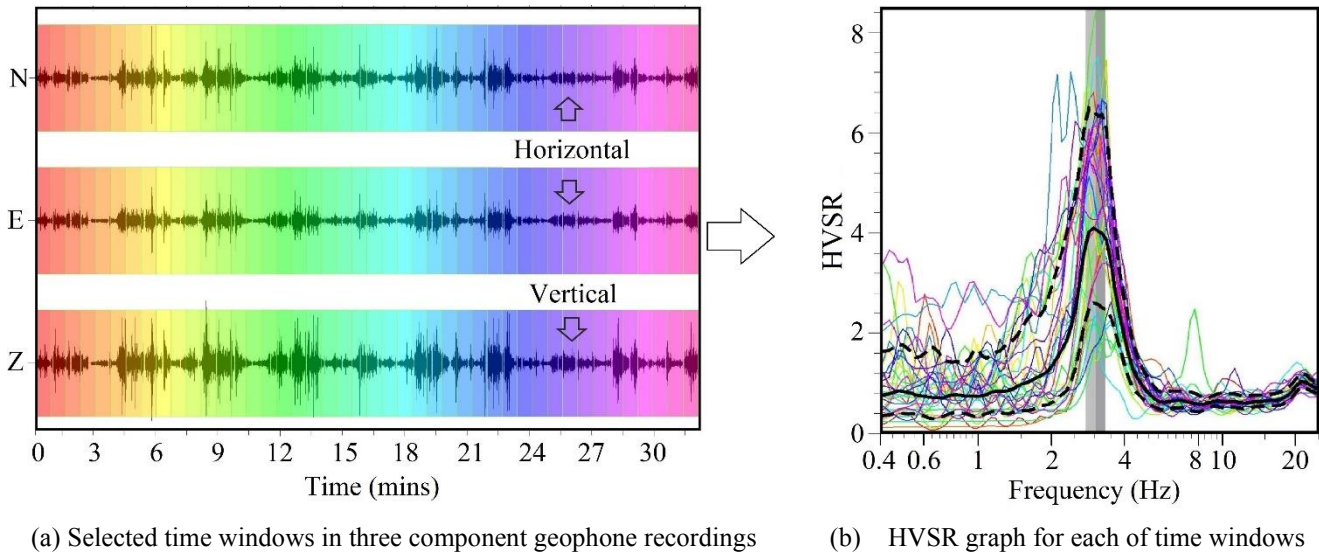


Fig. 1 HVSR measurements at the test site (S2)

*al.* 2019) for MAM respectively. The resulting dispersion curves were overlapped in a border frequency zone of 6 Hz and utilized for an inversion. The initial inversion model was constructed by one-third wavelength to the apparent depth and Rayleigh wave velocity transformation (Moon *et al.* 2017).  $V_s$  profiles generated by the least square method (Moon *et al.* 2019) are used as reference profiles for further comparison with ellipticity curve inversion results.

### 3.2. Horizontal-to-Vertical-Spectral-Ratio (HVSR)

The proposed empirical approach considers the HVSR method, popularized by (Nakamura 1989) and extensively used for two decades. The HVSR is a commonly used geophysical site investigation test that is aimed to characterize the soil (Pavel and Vacareanu 2015). This method assumes that there is a relationship between the HVSR of ambient noises and the fundamental frequency ( $f_0$  in Hz) of the soft sediment layer (Tokimatsu 1997, Bard 1999, Bonnefoy-Claudet *et al.* 2006, Hakimov *et al.* 2021). Ambient noise is low amplitude ground motion (usually on the order of 0.1-10  $\mu\text{m/s}$ ) caused by natural phenomena (earthquakes, wind, tides, rivers, rainfall) and human activities (roads, machines). Seismic noise associated with natural phenomena is mainly below 1 Hz, and human activities - above 1 Hz. The types of vibration waves covered by ambient noise contain a small portion of body waves (namely S-waves and P-waves) and rich in surface waves (Love waves and Rayleigh waves). Surface waves are dispersive waves, meaning that the surface wave's phase velocity is a function of frequency, i.e., the phase velocity is reversely proportional to frequency. Since there is a relationship between the dispersion curve and how  $V_s$  changes by depth in different soil layers, it can be utilized as a non-invasive method of assessing underground soil. At the site, the HVSR method consists of recording ambient noise over a short period using a three-component seismic station (Wathelet *et al.* 2020). All three-component ambient noise records (two horizontal and one vertical) are divided

into several time windows. For each time window, it is then transferred into the frequency domain by Fourier transform, transformed spectra then smoothed. For each predetermined window, the fractional relationship between averaged H to single V spectra is then calculated. A final HVSR graph is plotted by taking an average of all windows. These spectra show an amplitude peak at  $f_0$ , which correlates with the site's resonant frequency. Eq. (1) describes the correlation of  $f_0$  to soil parameters such as thickness ( $h$ ), shear wave velocity ( $V_s$ ), and in a single layer (Nakamura 1989)

$$f_0 = V_s/4h \quad (1)$$

In this study, seven single microseismic recordings were made for 30 minutes using a three-component geophone with a frequency of 4.5 Hz for each point. The distribution of measurements can be seen in Table 2. The data were collected and processed according to the recommendations by the SESAME project (2004). As an example, among seven test sites, Fig. 1 presents HVSR measurements at the Ang Mo Kio St. 24a (S2). Fig. 1(a) shows three component signals (two horizontal components and a vertical component) with time windows and corresponding HVSR of each time windows (Fig. 1(b)).

### 3.3. Ellipticity curve inversion

In 1D HVSR data, along with fundamental frequency and amplitude, is also utilized for calculating the ellipticity curve. The ellipticity curve information can be then applied to constrain the inversion using surface wave phase velocity curves (Fäh *et al.* 2009). Combined inversion of both dispersion curves taken from surface wave data and ellipticity curve can be used for determining bedrock (Fäh *et al.* 2008).

HVSR and ellipticity curves are close to each other because the contribution of the Rayleigh wave's fundamental mode to the HVSR model is much higher among the surface waves (Poggi *et al.* 2012). If a site's surface wave energy contribution consisted only of the

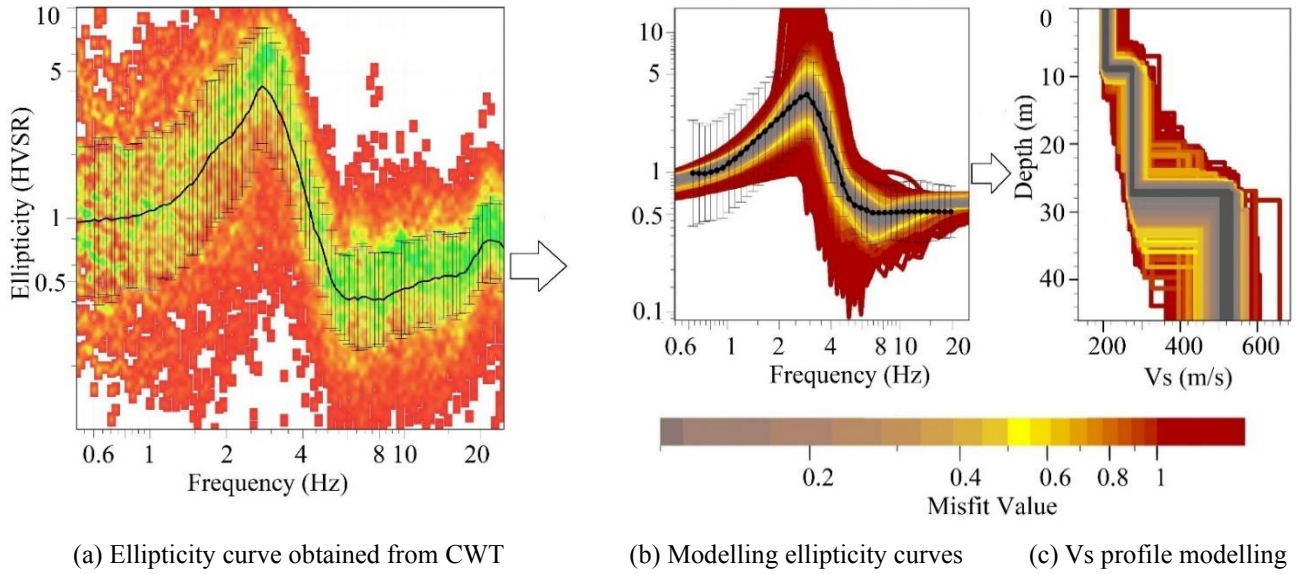


Fig. 2 Ellipticity inversion process at the test site (S2)

Rayleigh wave, then HVSR and Ellipticity curves would be exactly the same. However, considering HVSR as an ellipticity curve would be incorrect because the contribution of Rayleigh and Love waves is not constant even for the same site and differs with frequency (Hobiger *et al.* 2013). For that reason, the ellipticity curve of a site is needed to be estimated, although the main problem in extracting ellipticity curve from HVSR lies in adjusting the spectral recordings accordingly based on surface and body wave energy contributions.

Ellipticity curve can be typically estimated by using the RayDec method (Hobiger *et al.* 2009) or the method of elliptical retrieval, which utilizes a concept of a time-frequency analysis with a continuous wavelet transform (CWT) (Fäh *et al.* 2009, Poggi *et al.* 2012). In this study, the latter method is utilized in the Geopsy software (Fäh *et al.* 2009; Wathelet *et al.* 2020) to minimize the influence of horizontal S-wave (SH) and estimate the ellipticity curve from P-wave and vertical S-wave (SV) by CWT (Ullah *et al.* 2017). First, three-component signals are transformed into time-frequency (TF) representation using CWT separately. TF representation of two horizontal signals then merged via vector sum and TF representation of vertical signal would be considered as reference data in further estimations of Rayleigh wave contribution (Fäh *et al.* 2009; Poggi *et al.* 2012, Ullah *et al.* 2017). The procedure of CWT consists of time integration of measured signal ( $x(t)$ ) and wavelet function ( $\psi(t)(a, b)$ ) expressed in Eq. (2)

$$CWT\{x\}_{(a,b)} = \int_{-\infty}^{\infty} x(t) \psi^*(t)_{(a,b)} dt \quad (2)$$

Where  $\psi(t)_{(a,b)}$  is analyzing wavelet created from the mother wavelet function ( $\psi(t)$ ) by scaling and translation via parameters “a” and “b” by the Eq. (3)

$$\psi(t)_{(a,b)} = \frac{1}{\sqrt{|a|}} \psi\left(\frac{t-b}{a}\right) \quad (3)$$

Table 3 List of investigated sites using the HVSR method in the territory of Bukit Timah Granite in Singapore

Site ID	$f_0$ (Hz)	stdv( $f_0$ )	$A_0$	HVSR type
S1	3.4	0.22	5.7	clear peak
S2	3.0	0.24	4.5	clear peak
S3	2.7	0.14	3.7	double peak
S4	1.9	0.34	2.4	clear peak
S5	1.9	0.25	4.7	clear peak
S6	3.0	0.43	4.8	clear peak
S7	2.5	0.43	2.3	clear peak

Where the parameter “a” in the wavelet function is called the scale parameter and “b” is a shift of the wavelet function in time. The transformation process is repeated for all “a” and “b” values. Modified Morelet function is used as a mother wavelet in CWT (Fäh *et al.* 2009). Outputting time-frequency representation will result in a multiresolution: (1) good frequency/ poor time resolution at low frequencies; (2) poor frequency/good time resolution at high frequencies (Fäh *et al.* 2009, Ullah *et al.* 2017). Second, for statistically enhancing the reliability, TF representation is divided into a minute-long time windows (n) for further averaging the results (Poggi *et al.* 2012). Rayleigh waves’ vertical arrival is determined by assessing each time windows in vertical TF representations. Such time windows are further scanned for maxima at each frequency ( $f_{i,n}$ ). Horizontal amplitudes for each frequency are taken with a lag of quarter period ( $1/4f_{i,n}$ ) in comparison with vertical maxima time ( $t_{i,n}$ ). As a result, ellipticity curve is estimated as a ratio of horizontal amplitude to the vertical maxima and plotted in log scale. The same procedure is repeated for each frequency and time windows.

For the inversion procedure in the software, a global search method called the Neighborhood algorithm described by (Sambridge 1999, Wathelet 2005) is utilized. Given algorithm is classified as global search algorithm, meaning that the algorithm analyzes a whole parameter space

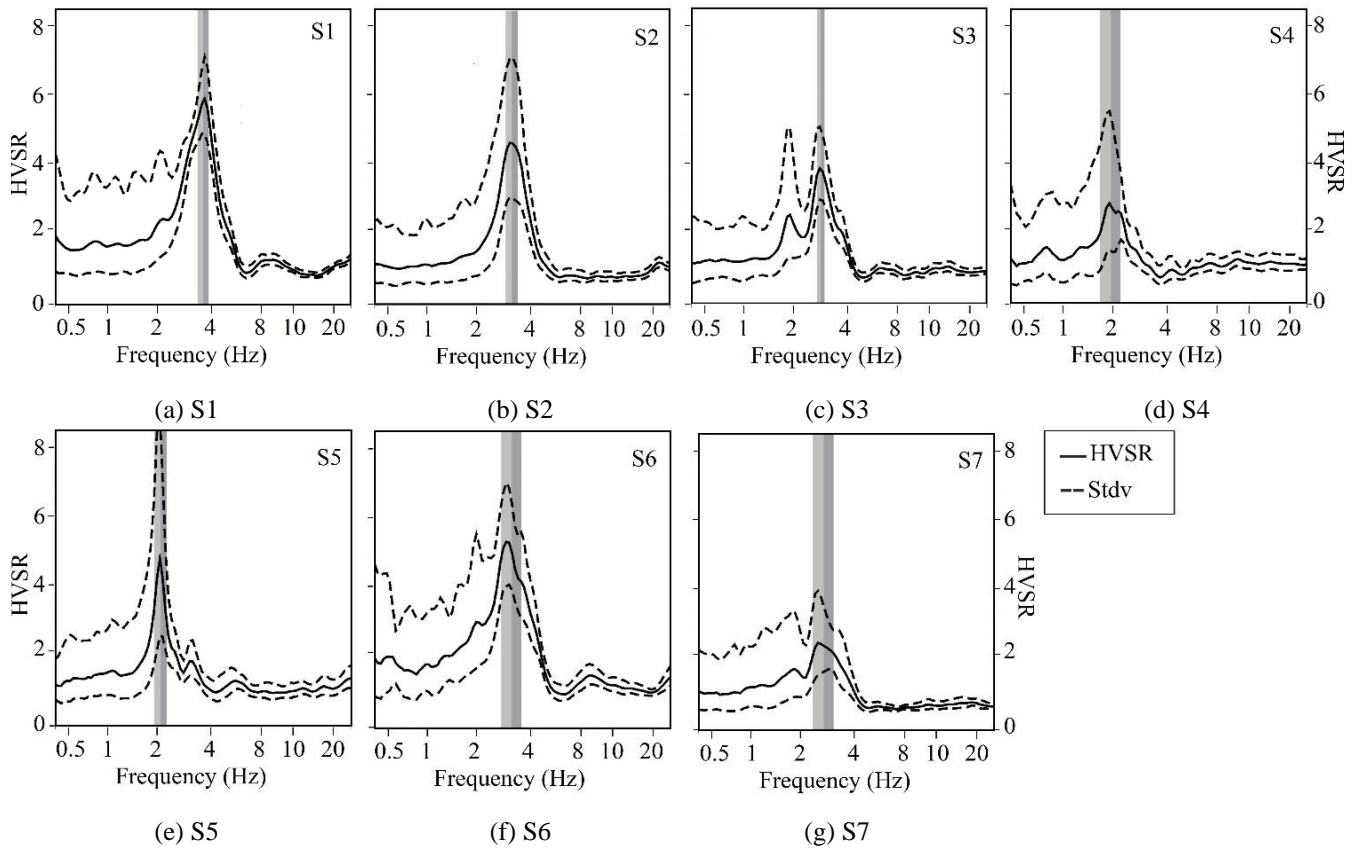


Fig. 3 HVSr results in seven test sites

including a possible thickness interval of each layer, and soil properties (density, Poisson's ratio, and minimum-maximum  $V_s$  and  $V_p$ ). After the analysis, the inversion algorithm will find the  $V_s$  models with the lowest misfit value. Inversion misfit is estimated using the following Eq. (4).

$$\text{Misfit} = \sqrt{\frac{1}{N} \sum_{i=1}^N \left( \frac{x_{di} - x_{ci}}{\sigma_i} \right)^2} \quad (4)$$

Where  $x_{di}$  and  $x_{ci}$  are reference and calculated velocities at frequency  $f_i$  respectively,  $\sigma_i$  is standard deviation,  $N$  is the number of samples.

Several previous studies (e.g., Dal Moro (2011), Ullah *et al.* (2017), Tumurbaatar *et al.* (2019)) highlighted that inversion of HVSr will reveal non-unique solutions. The global search algorithm itself might be time-consuming and might even not converge to the solution (Tumurbaatar *et al.* 2019). To overcome the non-uniqueness issues of inversion, additional constraints derived from geotechnical information would be required (Hobiger *et al.* 2013). In this study, borehole log data including geological information was utilized for constraining parameter space. In particular,  $V_s$  and layer depths were limited based on the known geology of layer and borehole log information.

Fig. 2 shows the ellipticity inversion process at the test site (S2). The resulting ellipticity curve from the time-frequency analysis can be seen in Fig. 2(a). Color dynamics from red to green show energy dynamics of HVSr

amplitude and the black line is the ellipticity curve that was statistically selected from the histogram. Fig. 2(b) illustrates ellipticity curves generated during the inversion and how well they fit with the ellipticity curve from Fig. 2(a). Grey lines and reddish-brown lines correspond to models with low misfits and high misfits, respectively. Fig. 2(c) illustrates inverted  $V_s$  profiles resulting from ellipticity curve inversion (Fig. 2(b)). The model with the lowest misfit value (grey) is selected for conducting further analysis.

## 4. Results

### 4.1. HVSr results

Fig. 3 presents HVSr curves of each test site using Geopsy software after the Rayleigh wave ellipticity (ellipticity curve) inversion process with ambient noises recorded. In the computation processes, three-component ambient noises were filtered out and were further smoothed using Konno-Omachi algorithm with the smoothing constant of 40. For each obtained HVSr,  $f_0$  and standard deviation (stdv) is estimated by considering the clear peaks in frequency spectra and taking an average of all time windows. The amplitude of the peak  $A_0$  is also measured as an indicator of the reliability of the estimate and the impedance contrast according to the SESAME project (2004). The average spectrum (black line) exhibits clear peaks (HVSr curves), black dashed lines as HVSr

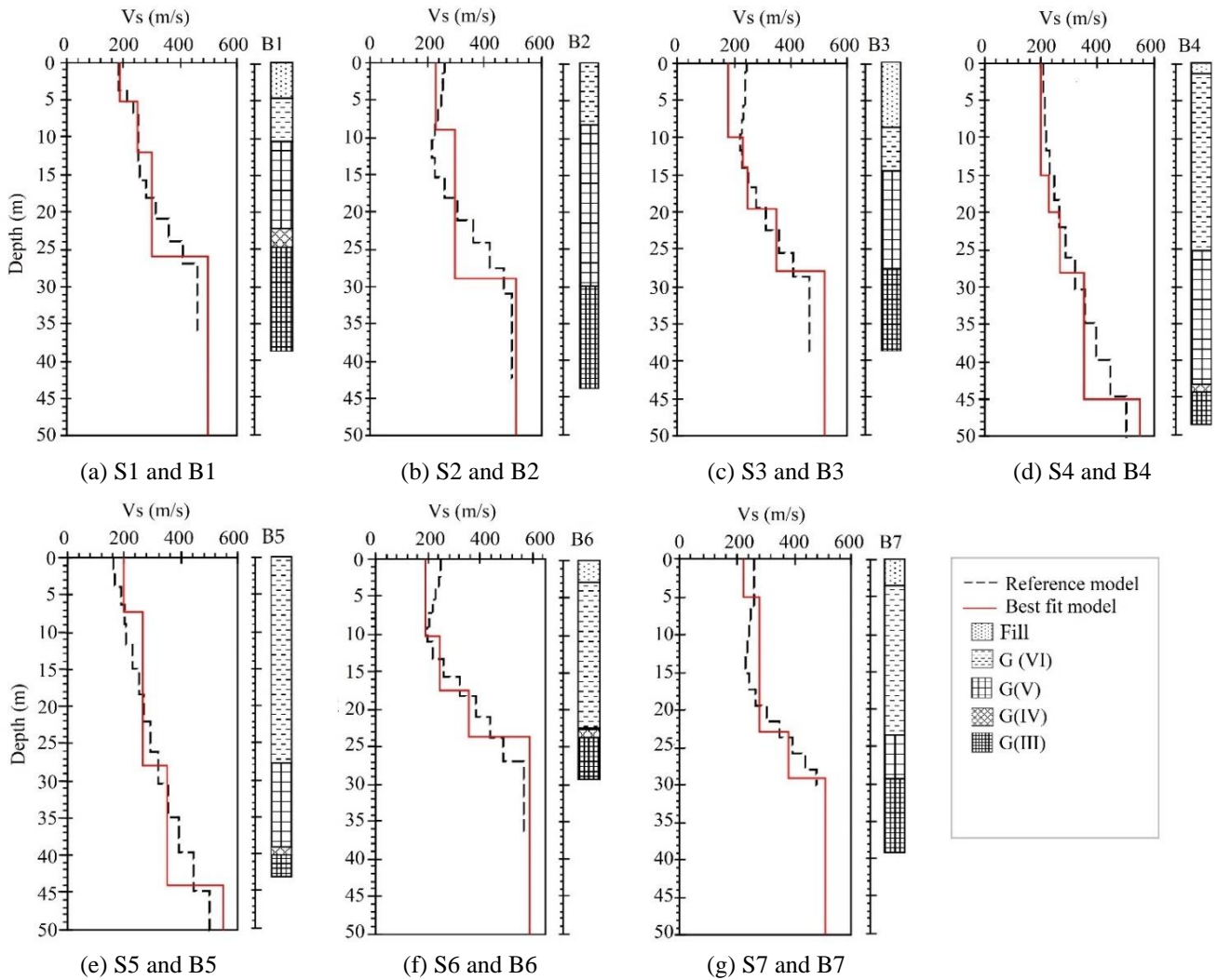


Fig. 4 The  $V_s$  profiles generated by Rayleigh wave ellipticity from the inversion of HVSRs (red line) on boreholes near and compared to the reference model from MASW and MAM (dashed line)

standard deviation (stdv), vertical grey marks as HVSR peak frequency  $f_0$  with stdv and its associated peak amplitude  $A_0$  for sites S1 to S7 (Fig. 3). The summary of results can be seen in Table 3.

The data is analyzed over a frequency range of 0.4 to 25 Hz considering the recommended criteria of clear and reliable peaks in following the SESAME project (2004). The HVSR results show a clear peak in the range of 1.9 Hz to 3.4 Hz (Table 3). For this class of sites, the average  $V_s$ , which was estimated after MASW and MAM results of the previous study (Moon *et al.* 2017, Moon *et al.* 2019), is in the range of 200-250 m/s for shallow and 450-650 m/s deep contrasts, suggesting that a large and sharp impedance contrast exists at the sediment (Bard 1999). Such clear peaks show frequencies greater than 1 Hz, corresponding to shallow sediment depth variation from 25 to 35 meters.

#### 4.2. Ellipticity curve inversion results

The ellipticity curve inversion of the Rayleigh wave was applied to determine shear wave velocity ( $V_s$ ) profiles using borehole data as an additional constraint (Fig. 4). We

established the maximum thickness of each layer, the P-wave and S-wave velocity, and density ranges by combining values from previous geophysical information (Moon *et al.* 2016) and calibration using HVSR measurements on boreholes data (Table 4). The range of the Poisson's ratio from 0.2 to 0.5 for all layers at each site was defined as the standard values for soils and rocks. To better limit the inversion and obtain reliable results, the average  $V_s$  estimated from the collected model  $V_s$  for shallow and deep contrasts were determined in the range of 200-250 m/s and 450-650 m/s, respectively. We calculated and compared the fundamental mode of the Rayleigh wave ellipticity curve at each site with the inverted part of the ellipticity curve obtained from measurements through misfit values. The S-wave velocity model corresponding to the minimum misfit value (the best model) is obtained (Fig. 4).

Fig. 4 reveals the  $V_s$  profiles of the test sites and corresponding borehole log data separately. Also, the reference  $V_s$  profiles obtained from the combination of MASW and MAM in the previous study (Moon *et al.* 2019) were compared with newly generated  $V_s$  profiles. Based on the borehole log composition and depth of each soil

Table 4 Intervals for model space investigation used in the HVSr curve inversion procedure of the study area

Layer	Thickness (m)	Vp (m/s)	Vs (m/s)	Density (kg/m <sup>3</sup> )
		min-max	min-max	min-max
1 <sup>st</sup>	0–10	320–450	180–260	1700–1900
2 <sup>nd</sup>	5–15	400–650	220–380	1800–2000
3 <sup>rd</sup>	10–30	450–800	250–450	2000–2100
4 <sup>th</sup>	25–50	600–1400	300–650	2200–2400

Table 5 Site Classification by HVSr and reference Vs profile data

Site ID	HVSr		Reference Vs profile	
	V <sub>S30</sub> (m/s)	Site class	V <sub>S30</sub> (m/s)	Site class
S1	280	D	275	D
S2	250	D	278	D
S3	253	D	271	D
S4	251	D	240	D
S5	252	D	228	D
S6	271	D	290	D
S7	270	D	281	D

formation, the Vs profiles are divided into three to four layers in the ellipticity curve inversion. Among inverted models, such an increased number of layers is observed in the sites (S3, S4, and S6). For all test sites, the Vs profiles modeled from the ellipticity curve and reference Vs profiles show a good agreement. In addition, soil/rock interface (i.e., depth of G III layer) in the sites (S1, S3, S4, S6, S7) fits well with increased Vs of the last layer of HVSr inverted profiles while the soil/rock interface in the sites (S2, S5) shows a 3-5 m difference. Newly generated Vs profiles are then also utilized for estimation of average Vs value for 30 meters.

#### 4.3. Site classification by V<sub>S30</sub>

Site amplification of earthquake caused by soft soil sediment and consequent site response are a drastic issue in seismic design and construction (Gautam *et al.* 2016, Maruyama and Sakemoto 2017, Zhao *et al.* 2017, 2018).

To evaluate and minimize potential earthquake hazard, seismic site classification has been conducted. Average Vs of 30 m (V<sub>S30</sub>) is conventionally utilized as an index of site characteristics in accordance with the National Earthquake Hazards Reduction Program (NEHRP) (BSSC 2001). The Vs profile inverted in the previous section is taken for estimation of V<sub>S30</sub> of each site. V<sub>S30</sub> were calculated following NEHRP guidelines and determined by the following Eq. (5)

$$V_{S30} = \frac{\sum_{i=1}^n d_i}{\sum_{i=1}^n (d_i/V_{S_i})} \quad (5)$$

Where  $d_i$  and  $V_{S_i}$  are depth and velocity of the  $i$ -th layer of soil in 30 m.

Table 5 shows the site classification of all seven test locations according to V<sub>S30</sub> values. For site classification, the V<sub>S30</sub> in the range of 180 to 360 m/s indicates Site Class D (stiff soil). For all the sites, the site classification based on the V<sub>S30</sub> obtained by the combination of MAM and

MASW and HVSr data reveal the same site class D with almost identical V<sub>S30</sub> value, which corresponds to the stiff soil class.

## 5. Conclusions

In this study, the shear wave velocity (Vs) profiles of seven locations in Bukit Timah Granite were generated using ellipticity curve inversion following the recommendations of earlier studies concerning additional constraints. A horizontal to vertical spectral ratio (HVSr) was also estimated for assessing the validity of data in accordance with SESAME project recommendations. A comparison of Vs profiles from the ellipticity curve with additional borehole constraint and the reference Vs profiles have indicated a reasonable trend in Vs profiles and similar V<sub>S30</sub> values. In accordance with National Earthquake Reduction Program (NEHRP) recommendations, V<sub>S30</sub> values in all seven test sites were estimated by the Vs profiles from the ellipticity curve inverted Vs and the reference Vs profiles all tested sites were classified as site class D (stiff soil). Also, soil/rock interface or bedrock depth in Bukit Timah Granite was estimated from newly generated Vs profiles using empirical approaches. Vs profile and borehole data have shown good agreement in soil/rock interface depth estimation. Thus, it can be stated that a single inversion of HVSr with parameter space constrain by borehole information can be a useful tool in site classification and Vs profile generation.

## Acknowledgements

The authors appreciate the financial support from the Nazarbayev University (Grant No. 110119FD4508).

## References

- Aki, K. (1957), "Space and time spectra of stationary stochastic waves, with special reference to microtremors", *Bull. Earthq. Res. Institute*, **35**, 415-456.
- Bard, P.Y. (1999), *Microtremor Measurements: A Tool for Site Effect Estimation?*, Balkema, Yokohama, Japan.
- Bard, P.Y. and SESAME-Team (2004), *Guidelines for the Implementation of the H/V Spectral Ratio Technique on Ambient Vibrations: Measurements, Processing, and Interpretations*, SESAME European Research Project Report: European Commission-Research General Directorate Project No. EVG1-CT-2000-00026 SESAME, 62. Available online: <ftp://ftp.geo.uib.no/pub/seismo/software/sesame/userguidelines/sesame-hv-user-guidelines.pdf> (accessed on 15 December 2020).
- Bonnefoy-Claudet, S., Cotton, F. and Bard, P.Y. (2006), "The nature of noise wavefield and its applications for site effects studies. A literature review", *Earth-Sci. Rev.*, **79** 205-227. <https://doi.org/10.1016/j.earscirev.2006.07.004>.
- BSSC (1999), *BS 5930: The Code of Practice for Site Investigations*, British Standard Institution, London, England.
- BSSC (2001), *The 2000 NEHRP Recommended Provisions for New Buildings and Other Structures, Part I (Provisions) and Part II (Commentary)*, FEMA, Washington, D.C.
- Dal Moro, G. (2011), "Some aspects about surface wave and

- HVSR analyses: A short overview and a case study”, *Bollettino di Geofisica Teorica ed Applicata*, **52**.  
<http://doi.org/10.4430/bgta0007>.
- Fäh, D., Stamm, G. and Havenith, H.B. (2008), “Analysis of three-component ambient vibration measurements”, *Geophys. J. Int.*, **172**, 199-213.  
<https://doi.org/10.1111/j.1365-246X.2007.03625.x>
- Fäh, D., Wathelet, M., Kristekova, M., Havenith, H.B., Knapmeyer-Endrun, B., Stamm, G., Poggi, V., Burjanek, J. and Cornou, C. (2009), *Using Ellipticity Information for Site Characterization*.
- Gautam, D., Forte, G. and Rodrigues, H. (2016), “Site effects and associated structural damage analysis in Kathmandu Valley”, *Nepal. Earthq. Struct.*, **10**, 1013-1032.
- Hakimov, F., Domej, G., Ischuk, A., Reicherter, K., Cauchie, L. and Havenith, H.B. (2021), “Site amplification analysis of Dushanbe City Area, Tajikistan to support seismic microzonation”, *Geosciences*, **11**(4), 154.  
<https://doi.org/10.3390/geosciences11040154>.
- Hobiger, M., Bard, P.Y., Cornou, C. and Le Bihan, N. (2009), “Single station determination of Rayleigh wave ellipticity by using the random decrement technique (RayDec)”, *Geophys. Res. Lett.*, **36**, L14303. <https://doi.org/10.1029/2009GL038863>.
- Hobiger, M., Cornou, C., Wathelet, M., Di Giulio, G., Knapmeyer-Endrun, B., Renalier, F., Bard, P.Y., Savvaidis, A., Hailemikael, S., Le Bihan, N., Ohrnberger, M. and Theodoulidis, N. (2013), “Ground structure imaging by inversions of Rayleigh wave ellipticity: Sensitivity analysis and application to European strong-motion sites”, *Geophys. J. Int.*, **192**, 207-229.  
<https://doi.org/10.1093/gji/ggs005>.
- Ku, T., Palanidoss, S., Zhang, Y., Moon, S.W., Wei, X., Huang, E., Kumarasamy, J. and Goh, K. (2020), “Practical configured microtremor array measurements (MAMs) for the geological investigation of underground space”, *Underground Space*.  
<https://doi.org/10.1016/j.undsp.2020.01.004>.
- Manandhar, S. and Cho, H.I. (2018), “New site classification system and design response spectra in Korean seismic code”, *Earthq. Struct.*, **15**(1), 1-8.  
<http://doi.org/10.12989/eas.2018.15.1.001>.
- Maruyama, Y. and Sakemoto, M. (2017), “Development of nationwide amplification map of response spectrum for Japan based on station correction factors”, *Earthq. Struct.*, **13**(1), 17-27. <https://doi.org/10.12989/eas.2017.13.1.017>.
- Moon, S.W. and Ku, T. (2016a), “Development of global correlation models between in situ stress-normalized shear wave velocity and soil unit weight for plastic soils”, *Canadian Geotech. J.*, **53**(10), 1600-1611. <https://doi.org/10.1139/cgj-2016-0015>.
- Moon, S.W. and Ku, T. (2016b), “Empirical estimation of soil unit weight and undrained shear strength from shear wave velocity measurements”, *5th International Conference on Geotechnical and Geophysical Site Characterisation, ISC 2016*, Sydney, Australia.
- Moon, S.W. and Ku, T. (2017), “Estimation of bedrock locations and weathering degree using shear wave velocity-based approach”, *Proceedings of the 19th International Conference on Soil Mechanics and Geotechnical Engineering (ICSMG)*
- Moon, S.W. and Ku, T. (2018), “Undrained shear strength in cohesive soils estimated by directional modes of in-situ shear wave velocity”, *Geotech. Geologic. Eng.*, **36**(5), 2851-2868.  
<https://doi.org/10.1007/s10706-018-0508-9>.
- Moon, S.W., Hayashi, K. and Ku, T. (2017), “Estimating spatial variations in bedrock depth and weathering degree in decomposed granite from surface waves”, *J. Geotech. Geoenviron. Eng.*, **143**.  
[https://doi.org/10.1061/\(ASCE\)GT.1943-5606.0001679](https://doi.org/10.1061/(ASCE)GT.1943-5606.0001679).
- Moon, S.W., Khan, Q. and Ku, T. (2016), Application of MASW methods for investigations of shear wave velocity in residual soils of Singapore, *In Geotechnical and Structural Engineering Congress 2016*, 1688-1699.  
<https://doi.org/10.1061/9780784479742.144>.
- Moon, S.W., Subramaniam, P., Zhang, Y., Vinoth, G. and Ku, T. (2019), “Bedrock depth evaluation using microtremor measurement: empirical guidelines at weathered granite formation in Singapore”, *J. Appl. Geophys.*, **171**.  
<https://doi.org/10.1016/j.jappgeo.2019.103866>.
- Nakamura, Y. (1989), “A method for dynamic characteristics estimation of subsurface using microtremor on the ground surface”, *Railway Technic. Res. Institute, Quarter. Reports*, **30**(1), 25-33.
- Park, C., Miller, R. and Xia, J. (1999), “Multichannel analysis of surface waves (MASW)”, *Geophysics*, **64**.  
<https://doi.org/10.1190/1.1444590>.
- Pavel, F. and Vacareanu, R. (2015), “Investigation on site conditions for seismic stations in Romania using H/V spectral ratio”, *Earthq. Struct.*, **9**(5), 983-997.  
<https://doi.org/10.12989/eas.2015.9.5.983>.
- Poggi, V., Fäh, D., Burjanek, J. and Giardini, D. (2012), “The use of Rayleigh-wave ellipticity for site-specific hazard assessment and microzonation: application to the city of Lucerne, Switzerland”, *Geophys. J. Int.*, **188**(3), 1154-1172.  
<https://doi.org/10.1111/j.1365-246X.2011.05305.x>.
- Sambridge, M. (1999), “Geophysical inversion with a neighbourhood algorithm-I. Searching a parameter space”, *Geophys. J. Int.*, **138**(2), 479-494.  
<https://doi.org/10.1046/j.1365-246X.1999.00876.x>
- Subramaniam, P., Zhang, Y. and Ku, T. (2019), “Underground survey to locate weathered bedrock depth using noninvasive microtremor measurements in Jurong sedimentary formation, Singapore”, *Tunnelling Underground Space Technol.*, **86**, 10-21.  
<https://doi.org/10.1016/j.tust.2019.01.005>.
- Tokimatsu, K. (1997), *Geotechnical Site Characterization Using Surface Geotechnical Engineering*, A A Balkema, Tokyo, Japan.
- Tumurbaatar, Z., Miura, H. and Tsamba, T. (2019), “Site effect assessment in Ulaanbaatar, Mongolia through inversion analysis of microtremor H/V spectral ratios”, *Geosci.*, **9**, 228.  
<https://doi.org/10.3390/geosciences9050228>.
- Ullah, I., Prado, R.L. and Lisa, M. (2017), “Single-station ellipticity retrieval and its joint inversion with dispersion curve, for a borehole test site”, *Arabian J. Geosci.*, **10**(14), 316.  
<https://doi.org/10.1007/s12517-017-3106-x>.
- Wathelet, M. (2005), *Array Recordings of Ambient Vibrations: Surface-Wave Inversion*, Universit'e de Li'ege, Belgium.
- Wathelet, M., Chatelain, J.L., Cornou, C., Di Giulio, G., Guillier, B., Ohrnberger, M. and Savvaidis, A. (2020), “Geopsy: A user-friendly open-source tool set for ambient vibration processing”, *Seismol. Res. Lett.*, **91**, 1878-1889.  
<https://doi.org/10.1785/0220190360>.
- Zhang, Y., Li, Y.E. and Ku, T. (2019), “Geotechnical site investigation for tunneling and underground works by advanced passive surface wave survey”, *Tunnelling Underground Space Technol.*, **90**, 319-329.  
<https://doi.org/10.1016/j.tust.2019.05.003>.
- Zhang, Y., Li, Y.E., Zhang, H. and Ku, T. (2019), “Near-surface site investigation by seismic interferometry using urban traffic noise in Singapore”, *Geophys.*, **84**(2), 1-43.  
<https://doi.org/10.1190/geo2017-0798.1>.
- Zhao, M., Gao, Z., Wang, L., Du, X., Huang, J. and Li, Y. (2017), “Obliquely incident earthquake for soil-structure interaction in layered half space”, *Earthq. Struct.*, **13**(6), 573-588.  
<https://doi.org/10.12989/eas.2017.13.6.573>.